Architectures for Vibration-Driven Micropower Generators

Paul D. Mitcheson, *Student Member, IEEE*, Tim C. Green, *Senior Member, IEEE*, Eric M. Yeatman, *Member, IEEE*, and Andrew S. Holmes, *Member, IEEE*

***Abstract*—Several forms of vibration-driven MEMS microgenerator are possible and are reported in the literature, with potential application areas including distributed sensing and ubiquitous computing. This paper sets out an analytical basis for their design and comparison, verified against full time-domain simulations. Most reported microgenerators are classified as either velocity-damped resonant generators (VDRGs) or Coulomb-damped resonant generators (CDRGs) and a unified analytical structure is provided for these generator types. Reported generators are shown to have operated at well below achievable power densities and design guides are given for optimising future devices. The paper also describes a new class—the Coulomb-force parametric generator (CFPG)—which does not operate in a resonant manner. For all three generators, expressions and graphs are provided showing the dependence of output power on key operating parameters. The optimization also considers physical generator constraints such as voltage limitation or maximum or minimum damping ratios. The sensitivity of each generator architecture to the source vibration frequency is analyzed and this shows that the CFPG can be better suited than the resonant generators to applications where the source frequency is likely to vary. It is demonstrated that mechanical resonance is particularly useful when the vibration source amplitude is small compared to the allowable mass-to-frame displacement. The CDRG and the VDRG generate the same power at resonance but give better performance below and above resonance respectively. Both resonant generator types are unable to operate when the allowable mass frame displacement is small compared to the vibration source amplitude, as is likely to be the case in some MEMS applications. The CFPG is, therefore, required for such applications. [944]**

***Index Terms*—Inertial-generators, microelectromechanical devices, micropower generators, self-powered systems, vibration-to-electric energy conversion.**

I. Introduction

PROSPECTS for wearable and ubiquitous computing will be greatly enhanced if miniature computing nodes requiring almost no maintenance can be provided [1]. In particular, these nodes should be self-powered in order to avoid the replacement of finite power sources [2], for example, by scavenging energy from the environment. With the ever reducing power requirements of both analog and digital circuits [3], power scavenging approaches are becoming increasingly realistic. One such approach is to drive an electromechanical converter from ambient motion or vibration. Fabrication of such power sources using MEMS technology is attractive in order to achieve small size and high precision.

Vibration-driven generators based on electromagnetic [4]–[7], electrostatic [8]–[10] or piezoelectric technologies [11], [12] have been demonstrated. While some of the reported generators have already been fabricated using MEMS techniques [7], [8], [10], [11], others have been made on a mesoscale with the intention of later miniaturizing the devices using MEMS [6], [13].

A general and unified analytical framework for such devices has not previously been established. We present in this paper such a unified framework, based on three fundamental generator classes. This analysis shows that previously reported MEMS generators have operated well below theoretically achievable power densities, and provides a methodology for designing optimized generators for particular applications.

We consider that any MEMS vibration-driven generator consists of a proof mass, m, moving within a frame. The operating principle is that the inertia of the mass causes it to move relative to the frame when the frame experiences acceleration. This relative displacement can then be used to generate energy by causing work to be done against a damping force, f, realized by an electric or magnetic field, or by straining a piezoelectric material. The mass is attached to the frame by a suspension which may be designed solely to constrain the motion of the mass, or to also create a resonant mass-spring system. The displacement of the mass from its rest position relative to the frame is denoted as $z(t)$. The absolute motion of the frame is $y(t)$ and that of the proof mass is $x(t) = y(t) + z(t)$. We consider harmonic source motion, so that $y(t) = Y_0 \cos \omega t$, Y_0 thus being the source motion amplitude. Equivalently, Z_0 is the amplitude of the mass-to-frame displacement. In a particular operating case, Z_0 will be mechanically constrained by the construction of the device. We define Z_l as a maximum possible Z_0 for a particular device. A generic model of a vibration-driven generator is shown in Fig. 1.

The upper limit on power generation for a given size of generator is ultimately dependent upon the nature of the damping force by which energy is extracted. This paper considers two resonant generators, one damped by a force which is proportional to velocity, the velocity-damped resonant-generator (VDRG), and one damped by a constant force, the Coulomb-damped resonant-generator (CDRG), and also one nonlinear generator, the Coulomb-force parametric-generator (CFPG). All three can be implemented in MEMS, using electromagnetics (for the VDRG) or electrostatics (for the other two).

Manuscript received October 14, 2002; revised May 9, 2003. This work was supported by the EPSRC and the DC Initiative (EU Framework V) under the ORESTEIA project. Subject Editor S. D. Senturia.

The authors are with the Department of Electrical and Electronic Engineering, Imperial College, London SW7 2BT U.K. (e-mail: pmitcheson@iee.org).

Digital Object Identifier 10.1109/JMEMS.2004.830151

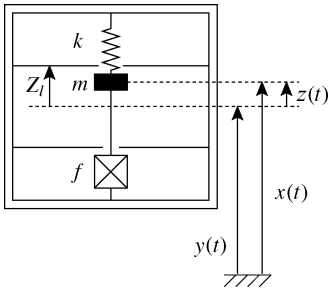

Fig. 1. Generic model of vibration-driven generator.

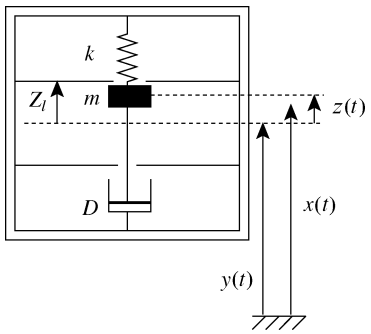

Fig. 2. Model of VDRG.

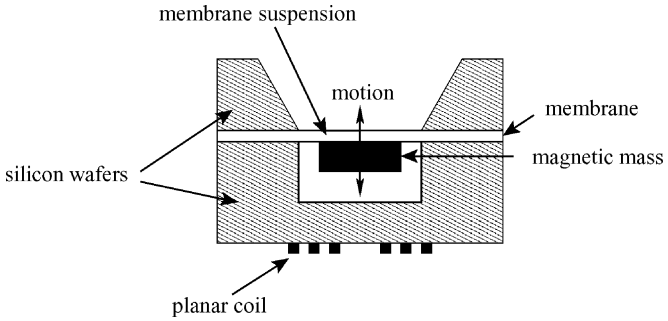

Fig. 3. Possible MEMS implementation of VDRG after [5].

Previously reported generators can be assigned to these classifications.

- Yates *et al.* [4], [5], [14], [15] of Sheffield University have constructed an electromagnetic MEMS VDRG, capable of generating 0.3 μW from a 4.4-kHz 500-nm input motion. Their device consists of a moving magnetic mass mounted on a flexure which allows a change of flux linkage with a coil deposited beneath the moving mass.
- Chandrakasan *et al.* of MIT have constructed both an electrostatic CDRG based on a comb-drive [8], [16], which generates 8 μW from a 2.5-kHz 500-nm input motion, and a larger electromagnetic VDRG [6], where they simulate approximately 400 μW root-mean-square (rms) power for an input motion which represents human walking.
- Li *et al.* of the Chinese University of Hong Kong have constructed and tested a MEMS electromagnetic VDRG [7]. They generate 40 μW from an 80-Hz 200-μm input vibration. They have successfully demonstrated data transmission powered by this source using a standard infrared transmitter running at a low duty cycle.
- White *et al.* of Southampton University have constructed a MEMS piezoelectric VDRG [11], [17], [18] capable of generating 2.2 μW from a 0.9-mm 80-Hz input motion.
- Tashiro *et al.* have constructed an electrostatic CDRG [19]. This is not a MEMS, or even miniature generator, weighing 0.64 kg.

Some of the previous work on microgenerators indicates that the power output of a vibration-driven device is proportional to $Y_0^2\omega^3 m$ [6], [15], [20]. This must be qualified by several factors. First, power will only increase as Y_0^2 if the maximum relative displacement Z_0 can increase in proportion to Y_0. However, Z_0 has a finite limit (Z_l), a key constraint in a MEMS application. Also, for the vibration source, Y_0 can be expected to drop with increasing ω. Another consideration is the ratio of the source frequency to the resonant frequency, ω_n, of the generator. This ratio is likely to vary with operating conditions and it is therefore useful to consider how it affects performance.

It will be shown that for idealized cases of all the architectures considered, the optimal output power can be derived as a function of Z_l/Y_0 and ω/ω_n and can be normalized to $Y_0^2\omega^3 m$. We have normalized using these values so that the graphs are general to all operating conditions. Also, by normalizing to this common base, fair comparisons between generators can be made. For each generator type, additional practical constraints and their effects on performance are then introduced.

The power generated by the resonant devices has been solved analytically for all operating modes. The results in each mode have been verified numerically with time-domain computer simulation for absolute value, optimality and validity under the constraints of that mode. The solution of the parametric generator is numeric from time-domain simulations.

II. Velocity-Damped Resonant Generators (VDRGs)

A. Ideal Case

A simple mechanical model of a VDRG is shown in Fig. 2, where energy is extracted by a damper whose force is proportional to $\dot{z}(t)$ with a constant of proportionality D. As a starting point, an idealized mass-spring system will be analyzed in which the damper represents the energy extraction mechanism.

Approximations to this type of damping have been used by Yates *et al.* [4], [5] and Amirtharajah *et al.* [6] and were implemented with moving magnets linking flux with stationary coils or vice-versa. A possible MEMS implementation of a VDRG based on [5] is shown in Fig. 3 and consists of two bonded silicon wafers. The lower wafer has a deposited coil and an etched well in which the mass can move. The upper wafer has a deposited membrane layer and an electroplated magnetic mass. The silicon is etched through to the membrane forming a spring.

The differential equation for the motion of the mass, m, relative to the frame is given by:

$$m\ddot{z}(t) = -kz(t) - D\dot{z}(t) - m\ddot{y}(t) \tag{1}$$

with k being the spring constant. Taking the Laplace transform of (1) and substituting in expressions for the normalized damping factor, $\zeta = (D/2m\omega_n)$, and the resonant frequency,

$\omega_n = \sqrt{k/m}$, the transfer function from frame motion, $Y(s)$, to the relative mass-to-frame motion, $Z(s)$, is obtained

$$\frac{Z(s)}{Y(s)} = \frac{-s^2}{s^2 + 2\zeta\omega_n s + \omega_n^2}. \tag{2}$$

The magnitude of the relative motion versus frequency is thus

$$\frac{Z_0}{Y_0} = \frac{\omega_c^2}{\sqrt{(1-\omega_c^2)^2 + (2\zeta\omega_c)^2}} \tag{3}$$

where $\omega_c = (\omega/\omega_n)$.

The energy dissipated per cycle is simply the distance integral of the damping force $D\dot{z}$ over a full cycle

$$\text{Energy per cycle} = 2D \int_{z=-Z_0}^{Z_0} \dot{z} dz. \tag{4}$$

Calculating this integral for the magnitude of Z_0 given by (3), and multiplying by frequency, gives an expression for the dissipated power, as has been reported in [14] (following the analysis of [21])

$$P = \frac{\zeta\omega_c^3 Y_0^2 \omega^3 m}{[1-\omega_c^2]^2 + [2\zeta\omega_c]^2}. \tag{5}$$

This suggests that for $\omega_c = 1$, the power extracted can be increased without limit by decreasing ζ. This occurs because of the following:

- the source motion has been assumed unconstrained, i.e., it is capable of supplying infinite power;
- there is no limit on Z_0, so at $\omega_c = 1$, $Zo \to \infty$ for $\zeta \to 0$;
- there is no parasitic damping present in the system.

All three of these factors will be addressed in Section V to show what can be achieved from practical generators operating at the resonant frequency.

Building on the previous analysis, it is possible to find the maximum power obtainable by first finding the optimal damping factor ζ_{opt}. This is given by the stationary point on $dP/d\zeta$, i.e.

$$\zeta_{\text{opt}} = \frac{1}{2\omega_c}|\omega_c^2 - 1| \tag{6}$$

(giving $\zeta_{\text{opt}} = 0$ for $\omega_c = 1$.)

The maximum power, $P_{\max}$, which can be dissipated in the damper, and thus converted into electrical energy, is then given by substituting (6) into (5)

$$P_{\max} = \frac{1}{4}\frac{\omega_c^2 Y_0^2 \omega^3 m}{|\omega_c^2 - 1|}. \tag{7}$$

The optimal value of ζ could violate constraints imposed by the system, the most fundamental of these being the displacement limit Z_l. The largest value of Z_l for currently reported MEMS microgenerators is 0.9 mm [11]. For given values of Y_0, ω, ω_n, and ζ, the unconstrained mass-to-frame amplitude Z_0 is given by a rearrangement of (3)

$$Z_0 = \frac{Y_0\omega_c^2}{\sqrt{(1-\omega_c^2)^2 + (2\zeta\omega_c)^2}}. \tag{8}$$

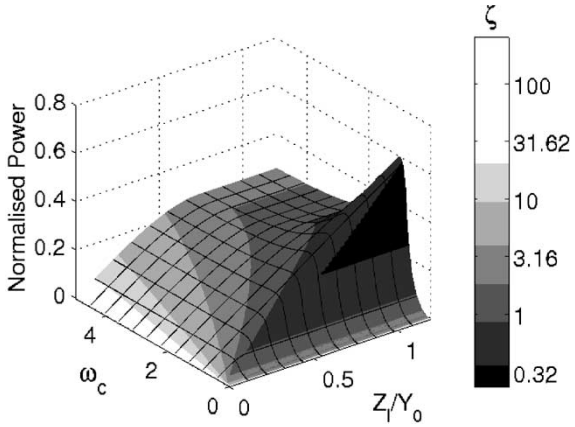

Fig. 4. VDRG maximum normalized power.

If the optimal value of ζ means that the Z_l limit is exceeded, a larger ζ should be chosen so that the amplitude is reduced to just below the limit and an unclipped resonant cycle is achieved. Power as a function of damping factor monotonically decreases each side of ζ_{opt} (for $\zeta_{\text{opt}} > 0$). Therefore the maximum (constrained optimal) power is achieved by operating as close to ζ_{opt} as possible while observing the displacement constraint. The constrained optimal damping factor $\zeta_{\text{opt}^{CZ}}$ is then given by a rearrangement of (3)

$$\zeta_{\text{opt}^{\text{CZ}}} = \frac{1}{2\omega_c}\sqrt{\omega_c^4\left(\frac{Y_0}{Z_l}\right)^2 - (1-\omega_c^2)^2}. \tag{9}$$

The power generated in this displacement constrained condition $P_{\max^{\text{CZ}}}$ is given by substituting (9) into (5)

$$P_{\max^{\text{CZ}}} = Y_0^2\omega^3 m\frac{1}{2\omega_c^2}\left(\frac{Z_l}{Y_0}\right)^2\sqrt{\omega_c^4\left(\frac{Y_0}{Z_l}\right)^2 - (1-\omega_c^2)^2}. \tag{10}$$

Note that at resonance, the device is always displacement limited, because the power, given by (5), increases for ζ tending to zero. Thus, the power P_{res} that can be generated at resonance is given by setting $\omega_c = 1$ in (10)

$$P_{\text{res}} = \frac{1}{2}Y_0^2\omega^3 m\frac{Z_l}{Y_0}. \tag{11}$$

The surface plot for optimal power generation by an ideal VDRG is shown in Fig. 4. As stated in the introduction, the power axis is normalized to $Y_0^2\omega^3 m$, and so is dimensionless. The height of the plot indicates the normalized power and the shading shows the damping factor ζ used at each point. This plot and equivalent plots for the VDRG assume that the damping factor is reoptimized for each operating point. This can be achieved by adjustment of the load electronics, whereas variation of ω_n would require the spring constant to be varied. The operating chart of Fig. 5 shows which analytic expressions for power generation are valid under which circumstances. The regions are

1) Device would generate more power if Z_0 could be increased beyond Z_l. Equation (10) applies.
2) Device operating optimally. Equation (7) applies.

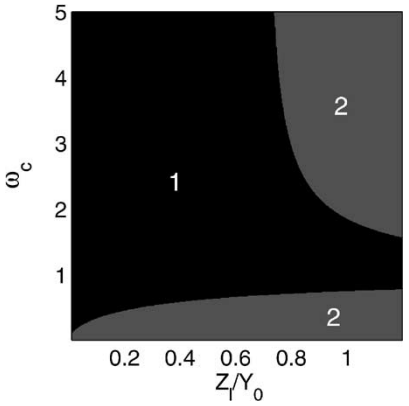

Fig. 5. VDRG idealized operating chart.

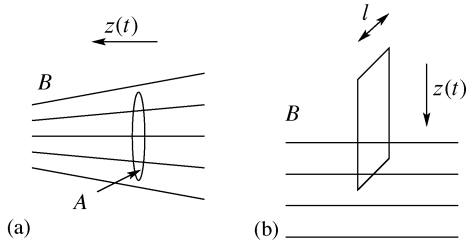

Fig. 6. Linearized magnetic models.

B. Hysteretic Damping

In hysteretic damping, also called rate-independent damping, the damping coefficient D is inversely proportional to frequency. This is often used to model hysteresis losses in structures, and has been suggested as an approximation for a piezoelectric generator [17]. Accurate modeling of piezoelectric generators results in a much more complex form [18].

If the damping coefficient is reoptimized for each operating frequency, the normalized output power for hysteretic damping is the same as for the VDRG as shown in Fig. 4.

C. Electromagnetic Implementation

The damper in a VDRG will typically be a moving magnet linking flux with a stationary coil, the latter having series inductance L and resistance. The operating principle is that voltage is induced in the coil due to the varying flux linkage, with the resultant currents causing forces which oppose the relative motion between the magnet and coil. In this analysis, we have lumped the coil resistance with the load resistance as R. The magnetic arrangement of Fig. 6(a) is the most likely for an electromagnetic generator, and has been used by Amirtharajah *et al.* [6] and Yates *et al.* [5]. This corresponds to a coil moving parallel to the diverging field of a permanent magnet. For the arrangement of Fig.6(a), if the gradient of magnetic field $(\mathrm{dB/dz}) = B'$ is constant across the plane of the coil, then the voltage induced in the coil is $NAB'\dot{z}$. In this case the force on the coil in the Laplace domain is given by $F(s) = s(NAB')^2 Z(s)/(R+sL)$, where N, A, and B are number of turns on the coil, coil area, and flux density, respectively. Fig. 6(b) shows a second possible linearized model, which is capable of providing a larger

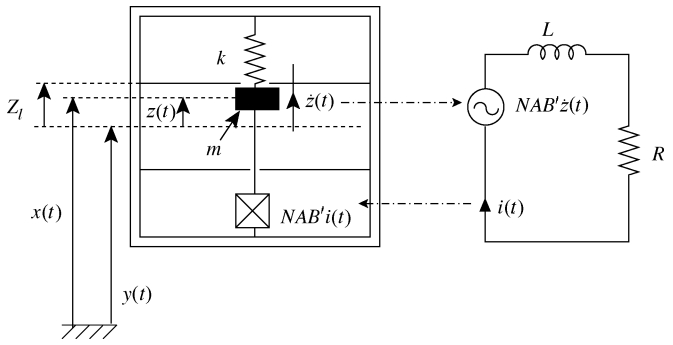

Fig. 7. Model of resonant electromagnetic generator.

damping force than Fig.6(a) because it contains a sharp transition from a uniform field region to a field-free region. This second arrangement is a popular model for analysis [4], [6], but corresponds less well with realizations that have been reported [4], [22]. In this case, the damping force is given by $F(s) = s(NBl)^2 Z(s)/(R + sL)$.

The differential equation of motion for these implementations is as (1), with the force on the moving magnet $f(t)$ taking the place of $D\dot{z}(t)$. The displacement transfer function for the magnetic generator of Fig. 7, for the arrangement of (6a), is found by taking the Laplace transform of this equation of motion and substituting in the expression for $F(s)$

$$\frac{Z(s)}{Y(s)} = \frac{-s^2 m}{s^2 m + \frac{s(NAB')^2}{R+sL} + k}. \tag{12}$$

If the ωL product is small relative to R, then the system can be mapped exactly onto a velocity-damped system with a damping coefficient $\zeta = \omega_c (NAB')^2/2\omega mR$. Amirtharajah [6] makes this assumption by stating that the electrical pole is faster than the mechanical pole. However, for an optimized generator under certain conditions, this may not be the case. To achieve the large damping required at high Y_0/Z_l ratios, the coil should have many turns, and thus will have a large self inductance. The resistance of the coil will increase if the wire conductor cross sectional area is not also increased, but the load resistance should be kept larger than the coil resistance to ensure high efficiency. The optimal damping factor may also require that the load impedance R is low.

If ωL is not neglected then the modulus of the displacement transfer function is found by taking the absolute value of (12)

$$\frac{Z_0}{Y_0} = \frac{m\omega^2\sqrt{R^2+\omega^2L^2}}{\sqrt{m^2R^2\left(\omega_n^2-\omega^2\right)^2+\omega^2\left(\left(NAB'\right)^2+mL\left(\omega_n^2-\omega^2\right)\right)^2}}. \tag{13}$$

Thus, the maximum velocity of the motion $z(t)$, V_0, is given by

$$V_0 = \frac{Y_0 m\omega^3\sqrt{R^2+\omega^2L^2}}{\sqrt{m^2R^2\left(\omega_n^2-\omega^2\right)^2+\omega^2\left(\left(NAB'\right)^2+mL\left(\omega_n^2-\omega^2\right)\right)^2}}. \tag{14}$$

The expression for the average power generated (i.e., dissipated in R) can then be found from $(\text{peakvoltage})^2/(2R)$, where the voltage is given by $NAB'V_0$

$$P = \frac{\frac{m^2\omega^6 Y_0^2 (NAB')^2 R}{2\omega_n^4}}{R^2\left(1-\omega_c^2\right)^2 m^2 + \omega^2\left(\left(\frac{NAB'}{\omega_n}\right)^2 + \left(1-\omega_c^2\right)mL\right)^2}. \tag{15}$$

It should be noted that at resonance, (15) reduces to that of a perfect velocity damper, because the inductor term falls out of the equation. However, at resonance Z_0/Y_0 is still dependent on L, as can be found by substituting $\omega = \omega_n$ into (13), giving

$$\frac{Z_0}{Y_0} = \frac{m\omega_n\sqrt{R^2+\omega_n^2 L}}{(NAB')^2}. \tag{16}$$

Reducing the inductance of the coil reduces the relative displacement of the mass at resonance. This is helpful in two respects. In the displacement constrained case ($Z_0 = Z_l$), for maximum realizable values of B', N, A and minimum realisable R, reducing L reduces the minimum Z_l/Y_0 for which the device can operate. In the unconstrained case, the parasitic damping will be amplitude dependent and is reduced by reducing the displacement amplitude. Consequently, an optimal electro-magnetic design operating around resonance should have a minimum inductance, but still have the required flux linkage to obtain the required damping factor. This can be achieved either by tuning out the inductance with a capacitor, or by using a unity power-factor power converter connected to the coil.

Below resonance, i.e., $\omega_c < 1$, every term on the denominator of (15) is positive, and so in order to maximize power generation, the value of L should be as small as possible or tuned out.

D. Practical Constraints

There are practical limits on the realization of the velocity damper which will now be considered. These are the following:

- maximum gradient and absolute value of magnetic field;
- maximum coil area;
- maximum number of coil turns achievable with an integrated inductor;
- minimum combined impedance of the coil and power converter input stage.

If the inductor is tuned out of the circuit, or the value of ωL is negligible compared to R, then the system is a perfect velocity damper. Using the model of Fig. 6(b), the damping factor is given by $((NBl)^2/2m\omega R)\omega_c$. The above factors then place a limit on the maximum realizable damping factor, $\zeta_{\max}$. An operating chart and optimal performance plot with constraints can now be plotted. These are shown in Figs. 8 and 9. As an example: we assume a flat, plated coil (Cu or Au) and a maximum coil area of 1 cm^2, for which a 10 turn coil of 1 Ω resistance is reasonable. Flux densities for permanent magnets do not generally exceed 1 T. We have chosen example values for mass and frequency of 2 g and 1.6 Hz, respectively.

The operating regions are as follows:

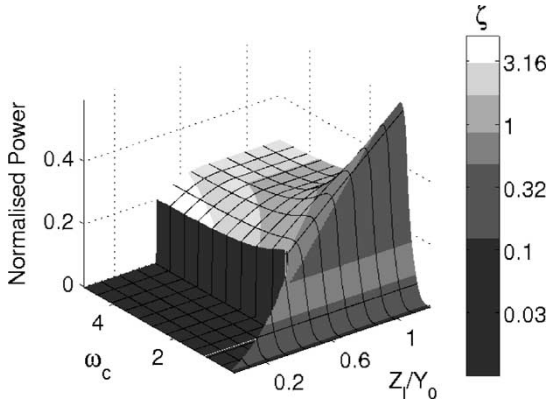

Fig. 8. VDRG with $\zeta_{\max}$ limit.

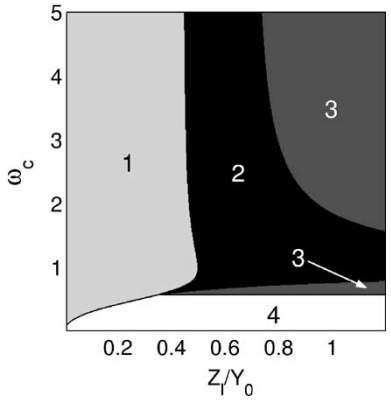

Fig. 9. VDRG operating chart with $\zeta_{\max}$ limit.

1) device unable to operate, the required ζ to meet the displacement constraint being greater than the system can achieve;
2) device operating at displacement limit. Equation (10) applies;
3) device operating optimally for the given value of ω_c. Equation (7) applies;
4) more power could be generated if the damping factor could be increased above the value of $\zeta_{\max}$. Equation (5) applies where $\zeta = \zeta_{\max}$.

III. Coulomb-Damped Resonant Generators (CDRGs)

A. Ideal Case

In the CDRG, energy is extracted by a damper which provides a constant force F in the direction opposing the motion. Coulomb damping is normally used when modeling the friction of a mass moving along a dry surface but can also be used to model certain electrostatic forces. A simple mechanical model of the system is shown in Fig. 10. Sliding capacitor plates operated in constant voltage and perpendicularly moving plates operated in constant charge produce constant forces with displacement [23], and are thus realizations of Coulomb dampers. Electrostatic approximations to CDRGs have been implemented by Meninger *et al.* [8] and Tashiro *et al.* [19] using MEMS comb-drives and a larger scale honeycomb structure respectively. These realizations are approximations because neither

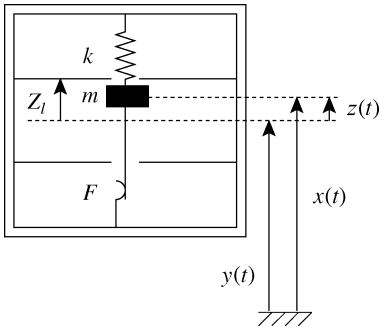

Fig. 10. Model of CDRG.

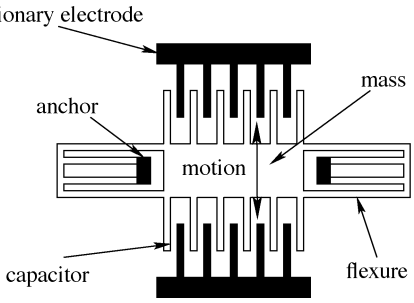

Fig. 11. Possible MEMS implementation of CDRG, after [8].

case implements purely constant voltage or constant charge cycles, and [19] has neither a perfect sliding or perpendicular motion. Fig. 11 shows a possible MEMS implementation of the device. A BSOI device layer is etched to define mass, suspension and anchors. The buried oxide is then wet etched to release the moving parts.

Although the CDRG oscillating system is nonlinear, a closed form solution is possible. Hartog [24] obtained an exact closed form solution to a force driven, Coulomb-damped mass-spring resonator by applying known boundary conditions to the motion. Levitan [25] obtained similar solutions for a support excited system using a Fourier series expansion. We have applied Hartog's method to the support excited motion, the result agreeing exactly with the solution given by Levitan.

According to this analysis, the transfer function from frame motion to relative mass-to-frame motion, is given by

$$\frac{Z_0}{Y_0} = \omega_c^2 \left[\frac{1}{\left(1-\omega_c^2\right)^2} - \left(\frac{F}{mY_0\omega^2\omega_c} U \right)^2 \right]^{\frac{1}{2}} \tag{17}$$

where $U = (\sin(\pi/\omega_c)/[1+\cos(\pi/\omega_c)])$ and F is the Coulomb force.

The energy dissipated is given by the force-distance product, and thus the power is

$$P = \frac{4Y_0 F \omega \omega_c^2}{2\pi} \left[\frac{1}{\left(1-\omega_c^2\right)^2} - \left(\frac{F}{mY_0\omega^2\omega_c} U \right)^2 \right]^{\frac{1}{2}}. \tag{18}$$

We can now extend this analysis as for the VDRG. The Coulomb force which optimizes the power output, F_{opt}, is given by $(dP/dF) = 0$

$$F_{\text{opt}} = \frac{Y_0\omega^2 m}{\sqrt{2}} \frac{\omega_c}{\left|\left(1-\omega_c^2\right)U\right|}. \tag{19}$$

The power $P_{\max}$ dissipated in the Coulomb damper with the optimal force applied is then obtained by substituting (19) into (18)

$$P_{\max} = \frac{\sqrt{2}}{\pi} Y_0^2 \omega^3 m \frac{\omega_c^3}{\left|\left(1-\omega_c^2\right)U\right|} \left[\frac{1}{\left(1-\omega_c^2\right)^2} - \frac{U}{\left(1-\omega_c^2\right)} \right]^{\frac{1}{2}}. \tag{20}$$

With this type of damping, the motion of the mass may become discontinuous. This is undesirable for a microgenerator as it makes the control and thus synchronization of the generator significantly more difficult. The requirement for nonstop motion is that the derivative of position is never zero within each half cycle. This is true if

$$F < \frac{Y_o \omega^2 m \omega_c^2}{\sqrt{\left(1+U^2\omega_c^2\right)\left(1-\omega_c^2\right)^2}}. \tag{21}$$

Note that this condition is only valid for $\omega_c > 0.5$. A method for calculating this limit is presented in [24].

It is possible for the value of optimal force calculated by (19) to be greater than that allowed by (21). This applies whenever $\omega_c < 0.72$. Under these conditions the optimal force is given by the limit of the inequality of (21), and the power generated is given by substituting (21) into (18)

$$P_{\max} = \frac{2Y_0^2\omega^3 m \omega_c^4}{\pi\sqrt{\left(1+U^2\omega_c^2\right)\left(1-\omega_c^2\right)^2}} \times \left[\frac{1}{\left(1-\omega_c^2\right)^2} - \frac{\omega_c U}{\sqrt{\left(1+U^2\omega_c^2\right)\left(1-\omega_c^2\right)^2}} \right]^{\frac{1}{2}}. \tag{22}$$

As for the VDRG, if the optimal force causes the displacement constraint to be exceeded, the force should be increased to preserve resonant motion. The optimal force that satisfies the displacement constraint, $F_{\text{opt}^{\text{CZ}}}$, is given by rearranging (17)

$$F_{\text{opt}^{\text{CZ}}} = \frac{Y_0\omega^2 m \omega_c}{|U|} \sqrt{\frac{1}{\left(1-\omega_c^2\right)^2} - \frac{1}{\omega_c^4}\left(\frac{Z_l}{Y_0}\right)^2} \tag{23}$$

and thus the maximum power under a displacement constraint $P_{\max^{\text{CZ}}}$ is now given by substituting (23) into (18)

$$P_{\max^{\text{CZ}}} = \frac{2\omega_c Y_0^2 \omega^3 m}{\pi|U|} \left(\frac{Z_l}{Y_0}\right) \sqrt{\frac{1}{\left(1-\omega_c^2\right)^2} - \frac{1}{\omega_c^4}\left(\frac{Z_l}{Y_0}\right)^2}. \tag{24}$$

It can be shown that at resonance (24) reduces to (11), i.e., optimal forms of the VDRG and the CDRG generate the same power at resonance.

Fig. 12 shows a surface plot of the power of the ideal Coulomb damper under optimized conditions, normalized as for the VDRG. The Coulomb force can be normalized to $Y_0\omega^2 m$; this has been done for Figs. 12, 14, and 16.

An operating chart is shown for this type of generator in Fig. 13. The regions are as follows:

1) Device not able to operate without stops in the motion—the force required to meet the displacement

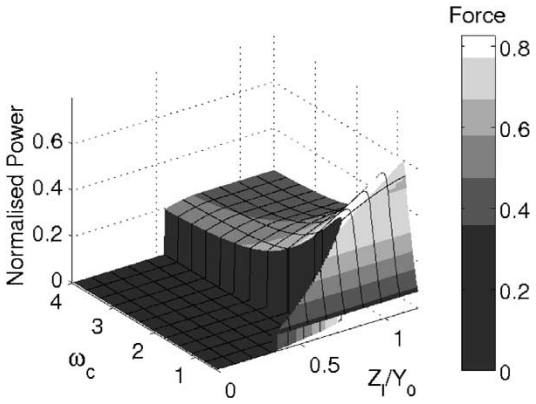

Fig. 12. CDRG maximum normalized power.

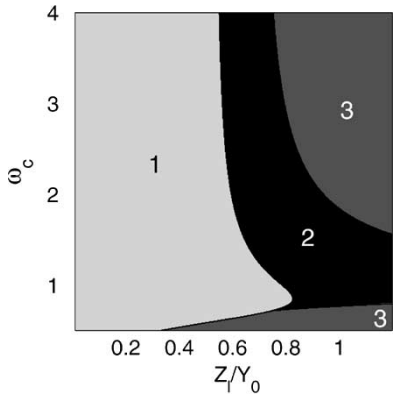

Fig. 13. CDRG idealized operating chart.

constraint (23) is greater than that for which smooth motion is valid (21).

2) For the given ω_c, more power would be generated if Z_l could be increased. Equation (24) applies.
3) Device operating optimally. Equations (20) and (22) apply for $\omega_c > 0.72$ and $\omega_c < 0.72$, respectively.

B. Practical Constraints

For a CDRG operated at constant charge, the voltage across the capacitor plates increases linearly with separation. If the voltage reaches the limit for the load electronics the holding force must be increased to reduce the range of travel sufficiently to keep the voltage within the limit.

The optimal output power for constant charge mode is shown in Fig. 14. The corresponding operating regions are as follows (see Fig. 15).

1) Device unable to operate without stops in the motion.
2) Power is limited by Z_l—(23) applies.
3) Device operating optimally. Equations (20) and (22) apply for $\omega_c > 0.72$ and $\omega_c < 0.72$, respectively.
4) Power constrained by maximum operating voltage. Here we have assumed a plate area of 1 cm^2, proof mass of 1 g, $\omega = 20\pi$, $Y_0 = 0.1$ mm. We have chosen 450 V as a reasonable limit for integrating power semiconductors and low power CMOS on the same wafer using SOI technology. It is possible that a device could be limited by electric field strength, but in the constant charge generator, the maximum voltage will appear across a relatively large gap.

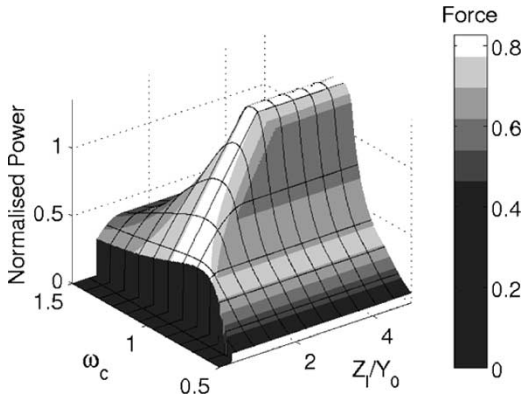

Fig. 14. CDRG optimal performance—perpendicular motion, constant Q.

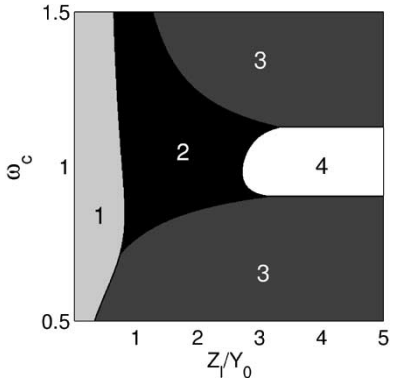

Fig. 15. CDRG operating chart—perpendicular motion, constant Q.

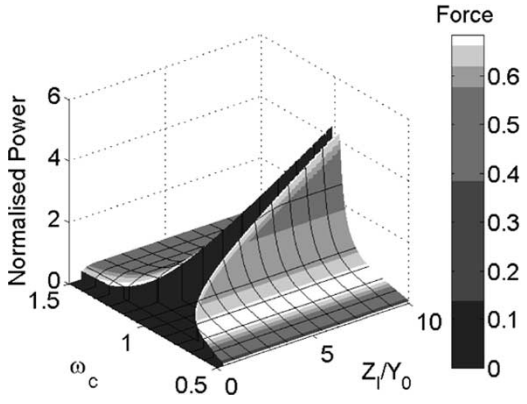

Fig. 16. CDRG optimal performance—sliding motion, constant V.

The optimal output power for constant voltage mode is shown in Fig. 16, and the corresponding operating regions in Fig. 17. This plot shows how the voltage constraint limits operation when the maximum available normalized force is, for example, 0.68:

1) device is unable to operate without stops in the motion;
2) power is limited by Z_l; (23) applies;
3) device operating optimally; (20) applies for $\omega_c > 0.72$ and (22) for $\omega_c < 0.72$;
4) more power would be generated if a greater Coulomb force could be realized;

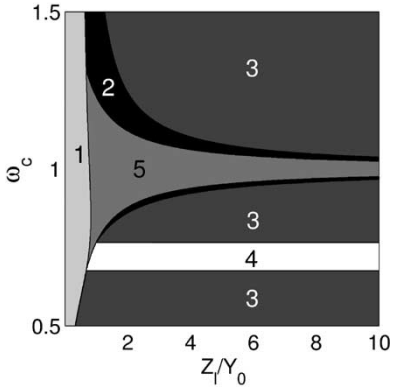

Fig. 17. CDRG operating chart—sliding motion, constant V.

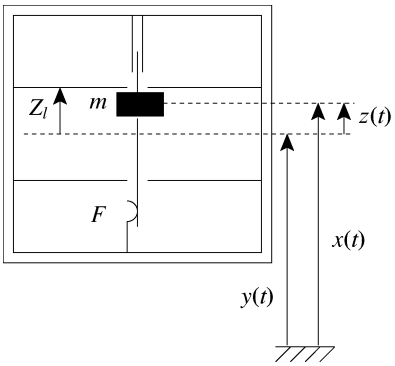

Fig. 18. Model of CFPG.

5) device is unable to operate—to meet the displacement constraint, the Coulomb force must be greater than that which can be provided by the system.

IV. Coulomb-Force Parametric Generators (CFPGs)

A. Ideal Case

The CFPG as shown in Fig. 18 is inherently nonlinear in nature. Rather than tuning the device to a resonant frequency by suspending the mass on a spring, the parametric generator only converts mechanical to electrical energy when the generator frame is at maximum acceleration. For the case in which Z_l/Y_0 is small, this corresponds to the mass snapping back and forth between the end-stops at the peak of the frame acceleration cycle. If Z_l/Y_0 is large, the mass must break away from the frame at an optimal acceleration and the energy must be extracted at the point of maximum separation. The snapping motion is illustrated in Fig.19. The proof mass is restrained by a holding force, and work is only done when the acceleration is great enough to overcome this force. As the mass has to move a finite distance, the breakaway force cannot be the value of $F_{\max}$ in the input motion, but must be some fraction, β, of it. This type of generator, as proposed in [26], has been fabricated at a meso-scale and is undergoing initial testing. Fabrication details and initial test results are reported in [13]. Fig. 20 shows a possible MEMS implementation. A variable-gap parallel-plate capacitor is formed between the BSOI device layer and a counterelectrode on the glass baseplate, with the minimum gap being

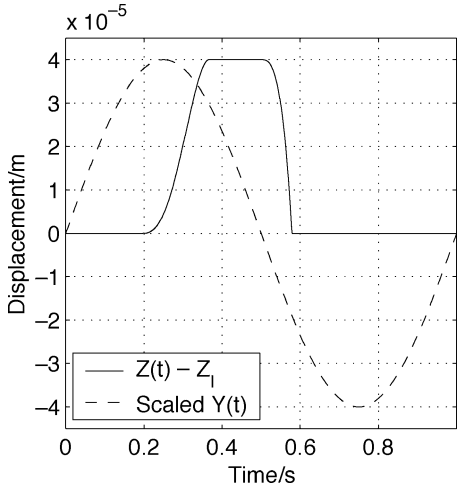

Fig. 19. Optimal parametric motion for $(Z_l/Y_0) = 0.01$.

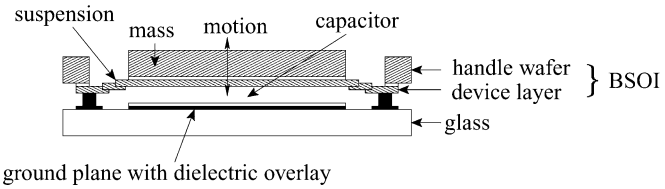

Fig. 20. Possible MEMS implementation of CFPG after [13].

defined by a dielectric overlay on the counterelectrode. The suspension is designed to present very low resistance out of plane but to be stiff in the in-plane directions.

The power generated by the parametric generator is given by the force-distance product, which, if energy is extracted for both directions of motion, is

$$P = 2\beta\left(\frac{Z_0}{Y_0}\right)\frac{Y_0^2\omega^3 m}{\pi}. \tag{25}$$

Optimizing this generator again requires the force-distance product to be maximized. A possible method is to write the equations of motion and find the time at which the separation is maximum, at which point the maximum work will have been done. From this, the work done and its maximum with respect to the break-away force can be found. Approximating the acceleration as uniform, we obtain

$$Z(t) - Z_l = Y_0\cos(\sin^{-1}\beta)[\omega t - \sin^{-1}\beta] - \frac{1}{2}\beta Y_0[\omega t - \sin^{-1}\beta]^2 + \beta Y_0 - Y_0\sin\omega t. \tag{26}$$

The derivative of (26) is similar to Kepler's equation and so has no closed form solution [27]. However, we can observe that the value of t for which $z(t)$ is maximum depends only on β and ω, and in fact can be written as $t_{\max} = (1/\omega)f(\beta)$.

Taking $2Z_0$ as the total displacement

$$2Z_0 = Y_0\cos(\sin^{-1}\beta)\left[f(\beta) - \sin^{-1}\beta\right] - \frac{1}{2}\beta Y_0\left[f(\beta) - \sin^{-1}\beta\right]^2 + \beta Y_0 - Y_0\sin f(\beta). \tag{27}$$

Thus, β is defined solely in terms of the ratio Z_0/Y_0 for sinusoidal input motion.

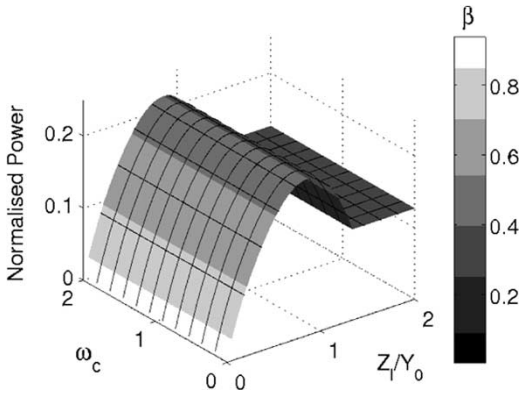

Fig. 21. CFPG maximum normalized power.

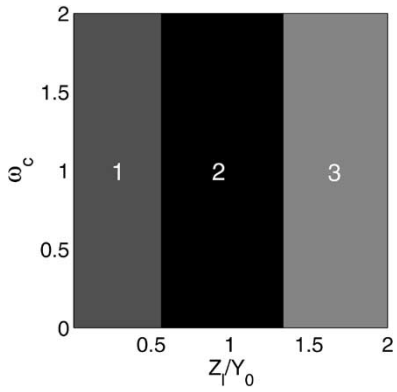

Fig. 22. CFPG idealized operating chart.

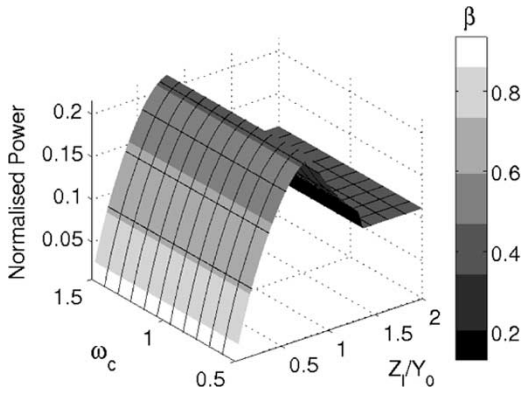

Fig. 23. CFPG optimal performance—perpendicular motion, constant Q.

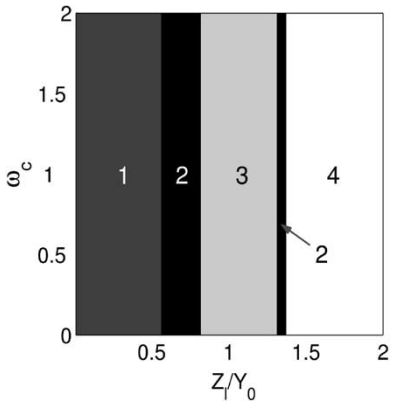

Fig. 24. CFPG operating chart—perpendicular motion, constant Q.

Simulations were run for the CFPG, altering β. These showed that the optimal β for maximum power generation is that which allows the mass to just move the full distance, $2Z_l$, until Z_l/Y_0 reaches a value of 1.286. Above this point, β should be fixed to maintain this ratio of Z_0/Y_0. However, an earlier limit is reached by the need for periodic operation, i.e., the need for $z(t)$ to return to $-Z_l$ within one cycle. This requirement also depends on whether energy is being extracted on the return stroke (double-sided operation), or not (single-sided operation).

The limit of possible double-sided operation occurs when the proof mass is unable to run from side to side symmetrically, i.e., it reaches the other side of the device at the point at which it must break away again to return. This limit is found from (26) by setting $\beta = 0$ and $t = (2\pi/\omega)$, giving $(Z_l/Y_0) \leq (\pi/2)$.

However, it can also be shown that single-sided operation gives more power than double-sided when $Z_l/Y_0 > 1.335$.

The maximum output power for the ideal parametric generator is shown in Fig. 21. Although ω_c has no significance because there is no resonant frequency, graphs are still plotted against ω_c to ease comparison with the other generators. The corresponding operating chart is shown in Fig. 22. The regions are as follows:

1) optimal double-sided operation;
2) β is reduced to allow double-sided operation, but double-sided operation is still better than optimal single-sided operation;
3) suboptimal single-sided operation (to allow periodic operation.)

B. Practical Constraints

As with the CDRG, the CFPG can use either sliding motion and constant voltage, or perpendicular motion and constant charge. For each case, the break-away force, and thus β, can be controlled by setting the initial voltage. For constant charge mode, the main constraint on optimal operation is likely to be the voltage capability of the output side power-processing circuitry. In this mode, the voltage increases from the start to the end of the cycle by the ratio of initial to final capacitance. For a comb style device, the limit on the applied voltage may restrict the Coulomb force to less than that needed for optimal operation.

The power output for a constant charge mode CFPG is shown in Fig. 23, and the corresponding operating chart is shown in Fig. 24. The operating regions are as follows.

1) Optimal double-sided mode.
2) β reduced to enable double-sided operation.
3) Double-sided operation with β reduced to stay within the voltage limit. The plot is for $m = 1$ g, $Y_0 = 0.5$ mm, $f = 1$ Hz, Plate Area $= 1$ cm^2, $V_{\text{limit}} = 110$ V. Although the output side power electronics could be designed to block more than 120 V, this limit has been chosen to illustrate the effect more clearly.
4) Device in voltage limit for output-side electronics. Operation single-sided.

The power output for a constant voltage mode CFPG is shown in Fig. 25. The graph is plotted for the example of a maximum

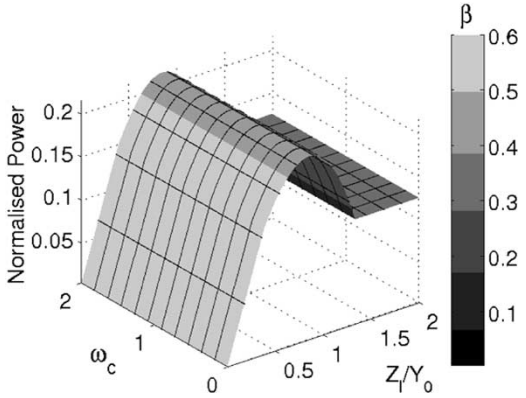

Fig. 25. CFPG optimal performance—sliding motion, constant V.

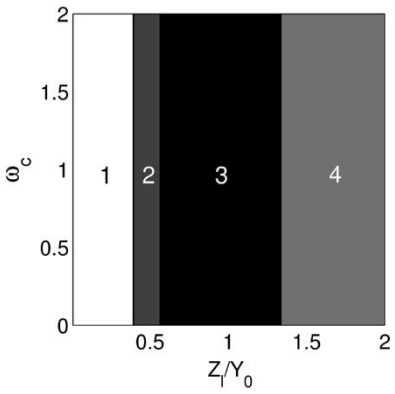

Fig. 26. CFPG operating chart—sliding motion, constant V.

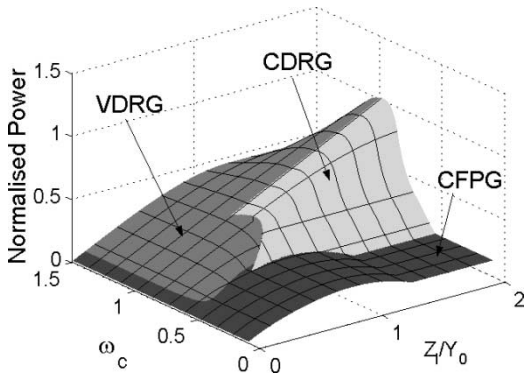

Fig. 27. Generator architecture comparison.

achievable β of 0.6. The corresponding operating chart is shown in Fig. 26. The operating regions are as follows:

1) device in voltage limit; β at the limit of 0.6;
2) optimal double-sided operation—the device is operating optimally on each stroke;
3) suboptimal double-sided operation;
4) single-sided operation.

V. Discussion

A. Comparison of Idealized Generator Types

The graph of Fig. 27 shows which optimized generator architecture can produce the most power as a function of operating condition. As can be seen, the CFPG is superior at low ratios of Z_l/Y_0, and for frequencies well below the resonant frequency of the resonant generators. The CDRG is superior below resonance (except for low Z_l/Y_0 values) and the VDRG is superior above resonance. The two give the same performance at resonance.

Applications for micropower generators fall into two main categories—devices powered by human body motion, and those powered by vibration of machinery. Body motion (of limbs or the cardiovascular system) is of low frequency and relatively high amplitude compared to the dimensions of reported generators, whereas the vibrations of machinery are generally of high frequency and low amplitude. Thus, the parametric generator is suitable for generating power from the human body, while resonant generators are appropriate for generating power from machinery (at least for a narrow source frequency range).

B. Parasitic Damping

Parasitic damping effects, such as air resistance or hysteresis loss in the suspension, are difficult to estimate for a general topology, being dependent upon materials, structure, and maximum displacement. Consequently, the above analysis has not included parasitic damping. However, the limits on the absolute validity of the results will now be discussed.

Williams *et al.* [15] state that for their fabricated generator, the parasitic damping coefficient, ζ_p, due to the air and spring hysteresis is of the order of 0.0037, while the measured value for their device operated in vacuum is 0.0023. Optimal operation of this device (a VDRG) requires an electrical damping factor $\zeta_e = (Y_0/2Z_l)$ ((3) with $\omega_c = 1$.) For electrical damping to dominate in the vacuum case (e.g., $\zeta_e \geq 10\zeta_p$) requires $(Z_l/Y_0) < 20$.

The maximum value of Z_l currently reported for MEMS engineered microgenerators is 0.9 mm [11], while vibration source amplitudes as low as 3 nm have been reported [8]. Consequently, parasitic damping may be significant in some situations.

For an optimized generator, the parasitic damping could be significantly reduced over the design of [4]. For example, Nguyen states that air damping is the dominant parasitic for micro-mechanical resonators for Qs of up to 50 000, beyond which hysteretic damping of the material is the dominant factor [28]. Elimination of air damping by, e.g., vacuum packaging in this case would, therefore, yield a residual damping coefficient of 2×10^{-5}.

The power generated by a resonant VDRG with parasitic damping can be written, as in [20] as

$$P = \frac{\zeta_e \omega_c^3 Y_0^2 \omega^3 m}{[1-\omega_c^2]^2 + [2\zeta_t \omega_c]^2} \tag{28}$$

where $\zeta_t = \zeta_e + \zeta_p$. Should the parasitic damping be significant, the electrical damping factor should be reoptimized. For a velocity damper, this optimal ζ_e is again given by the stationary point on $dP/d\zeta_e$

$$\zeta_e = \frac{1}{2\omega_c}\sqrt{1 - 2\omega_c^2 + \omega_c^4 + 4\omega_c^2\zeta_p^2}. \tag{29}$$

An equivalent optimal damping factor can be obtained for the Coulomb damped case in the same fashion. Levitan [25]

described a solution for a support excited system with combined Coulomb and viscous damping. However, the analysis will not be presented here.

C. Vibration Source Limitations

As stated previously, a microgenerator is likely to have little effect on a vibration source it is attached to. This effect can be quantified by considering the source to have an internal damper analagous to the output impedance of a voltage source. Modeling of such a system suggests that if the power extracted by the microgenerator is more than 1% of the maximum output of the source, the effect of the source limitation on performance becomes significant.

D. Expected Power Densities

The ultimate limiting factor for an inertial microgenerator is size, which limits both mass and travel. Since the power is linearly proportional to m and to Z_l, the power is maximized for a mass taking up half the device volume. This can be justified as follows.

In the direction of motion, the overall device dimension, l, must be divided between the range of internal travel, $2Z_l$, and the dimension of the mass in that direction, Z_m. Since the output power is proportional to the product of mass and $2Z_l$ (for a given operating condition), power will be maximized for $2Z_l = Z_m$, i.e., for the mass taking up half the space. Power will now be proportional to l^2, and to the other two spatial dimensions. This suggests that micro-generator power is proportional to $\text{volume}^{4/3}$.

The power generation values which have been discussed so far are the limits of the power that can be coupled into the generator damper. However, the electrical power which can be generated will be some proportion of that coupled power, due to various losses. These losses include the following.

- Parasitic Damping: reduces the maximum electrical power as discussed above.
- Charge Leakage: For an electrostatic generator charge will leak from the moving plates during the generation cycle due to finite impedance between them. This reduces the Coulomb force, and thus the power generated.
- Operational Overhead: Some power will be consumed by the generator control electronics.
- Electrical Losses: These losses will include conduction and switching losses.

We define the performance metric for microgenerators as the product of two terms: the coupling effectiveness (coupled power/maximum possible coupled power) and an efficiency (useful power output/coupled power). Coupled power is the power dissipated in the generator's damper, and useful power output is the power available to drive external circuitry after suitable power processing.

Taking for ρ the density of gold, being the highest for a MEMS material, and a generator effectiveness of 100% and a volume of 1 cm^3, typical expected power densities for microgenerators are as follows:

For a human powered application (with movements at 1 Hz and 5 mm amplitude) we estimate 4 $\mu\text{W}/\text{cm}^3$, using a parametric generator. This will be sufficient for some autonomous sensor applications.

For a machine powered application (with vibrations of 2 nm at 2500 Hz), using a resonant generator, we estimate power densities closer to 800 $\mu\text{W}/\text{cm}^3$.

Where the relevant information is available (i.e., Y_0, ω, Z_l, m), the performance of some previously reported generators can now be discussed. The electrostatic generator presented in [8] achieves an effectiveness of 0.32%. The electromagnetic generator of [5] achieves an effectiveness of 6% and the electromagnetic generator of [20] achieves an effectiveness of 0.4%. These values correspond to the devices operating at the resonant frequency. Consequently, there is much potential for improvement in future devices.

VI. Conclusion

In this paper, analysis of three microgenerator architectures has been presented with a view to understanding the relative merits of each, and in order to find optimal architectures for maximal power generation under the different operating constraints of displacement and normalized frequency. Analysis has been verified by time-domain simulation. It has been shown that under operating conditions of known Z_l/Y_0 and ω/ω_n ratios, the expressions for the power generated for all architectures can be normalized to $Y_0^2\omega^3 m$. For ideal implementations, the following conclusions hold:

- the CFPG produces the most power where $(Z_l/Y_0) < 0.1$;
- the VDRG is superior above the resonant frequency when $(Z_l/Y_0) > 0.1$;
- the CDRG is superior below but near the resonant frequency when $(Z_l/Y_0) > 0.1$;
- generators only benefit from operating at or near resonance when $Z_l > Y_0$;
- it is not possible to operate a CDRG at low Z_l/Y_0 ratios and maintain smooth motion of the proof mass, making the generator control and synchronization difficult.

Additional conclusions can be drawn when practical implementation issues are taken into account:

- it is not possible to operate the VDRG for small Z_l/Y_0 ratios. At some value of Z_l/Y_0, the required damping factor will become unrealisable due to limits on minimum coil and load impedance and maximum achievable magnetic field strength;
- at the resonant frequency, the coil inductance of the resonant electromagnetic generators has no effect upon performance, because the system simplifies exactly to a perfect VDRG.

The limiting factor for an inertial microgenerator is size, which limits both mass and travel. We would expect typical power densities of a few $\mu\text{W}/\text{cm}^3$ for human body motion and hundreds of $\mu\text{W}/\text{cm}^3$ for machine powered applications.

Acknowledgment

The authors would like to thank Dr. P. Miao of Imperial College for his helpful contributions on generator realization and to Dr. B. H. Stark for helpful discussions.

REFERENCES

[1] J. M. Rabaey, M. J. Ammer, J. L. da Silva, Jr., D. Patel, and S. Roundy, "Picoradio supports ad hoc ultra-low power wireless networking," *IEEE Comput. Mag.*, pp. 42–48, July 2000.

[2] T. Starner, "Human powered wearable computing," *IBM Syst. J.*, vol. 35, no. 3/4, pp. 618–629, 1996.

[3] E. A. Vittoz, "Low-power design: ways to approach the limits," in *Proc. IEEE Int. Solid State Circuits Dig. Tech. Papers*, Feb. 1994, pp. 14–18.

[4] C. B. Williams and R. B. Yates, "Analysis of a micro-electric generator for microsystems," in *Proc. Solid-State Sensors and Actuators, 1995 and Eurosensors IX. Transducers '95*, vol. 1, 1995, pp. 369–372.

[5] S. Shearwood and R. B. Yates, "Development of an electromagnetic micro-generator," *Electron. Lett.*, vol. 33, pp. 1883–1884, Oct. 1997.

[6] R. Amirtharajah and A. P. Chandrakasan, "Self-powered signal processing using vibration-based power generation," *IEEE J. Solid State Circuits*, vol. 33, pp. 687–695, May 1998.

[7] W. J. Li, G. M. H. Chan, N. N. H. Ching, P. H. W. Leong, and H. Y. Wong, "Dynamical modeling and simulation of a laser-micromachined vibration-based micro power generator," *Int. J. Nonlinear Sci. Simulation*, vol. 1, pp. 345–353, 2000.

[8] S. Meninger, J. O. Mur-Miranda, R. Amirtharajah, A. P. Chandrakasan, and J. H. Lang, "Vibration-to-electric energy conversion," *IEEE Trans. VLSI Syst.*, vol. 9, pp. 64–76, Feb. 2001.

[9] ——, "A micropower programmable DSP powered using a MEMS-based vibration-to-electric energy converter," in *Proc. IEEE Int. Conf. Solid State Circuits*, 2000, pp. 362–363.

[10] S. Roundy, P. K. Wright, and K. S. Pister, "Micro-electrostatic vibration-to-electricity converters," in *Proc. 2002 ASME Int. Mechan. Eng. Congress and Exposition*, New Orleans, LA, Nov. 2002.

[11] N. M. White, P. Glynne-Jones, and S. Beeby, "A novel thick-film piezoelectric micro-generator," *Smart Mater. Struct.*, vol. 10, pp. 850–852, Aug. 2001.

[12] M. J. Konak, I. G. Powlesland, S. P. van der Velden, and S. C. Galea, "A self-powered discrete time piezo-elecric vibration damper," *SPIE—Proc. Int. Soc. Opt. Eng.*, pp. 270–279, 1997.

[13] P. Miao, A. S. Holmes, E. M Yeatman, T. C. Green, and P. D. Mitcheson, "Micro-machined variable capacitors for power generation," in *Proc. Electrostatics '03*, Edinburgh, U.K., Mar. 2003.

[14] C. B. Williams, R. C. Woods, and R. B. Yates, "Feasibility study of a vibration powered micro-electric generator," in *Proc. IEE Colloq. Compact Power Sources (Digest No. 96/107)*, May 1996, pp. 7/1–7/3.

[15] C. B. Williams, S. Shearwood, M. A. Harradine, P. H. Mellor, T. S. Birch, and R. B. Yates, "Development of an electromagnetic micro-generator," *IEE Proc. Circuits, Devices and Syst.,* , vol. 148, no. 6, pp. 337–342, Dec. 2001.

[16] S. Meninger, J. O. Mur-Miranda, R. Amirtharajah, A. Chandrakasan, and J. Lang, "Vibration-to-electric energy conversion," in *Proc. 1999 Int. Symp. Low Power Electron. Design*, Aug. 1999, pp. 48–53.

[17] P. Glynne-Jones, S. Beeby, and N. M. White, "Toward a piezoelectric vibration-powered microgenerator," *Sci., Measure. Technol.*, vol. 48, pp. 68–72, Mar. 2001.

[18] P. Glynne-Jones, S. P. Beeby, E. P. James, and N. M. White, "The modeling of a piezoelectric vibration powered generator for microsystems," in *Proc. 11th Int. Conf. Solid-State Sensors and Actuators, Transducers '01 and Eurosensors XV*, Munich, Germany, June 2001, pp. 46–49.

[19] R. Tashiro, N. Kabei, K. Katayama, Y. Ishizuka, F. Tsuboi, and K. Tsuchiya, "Development of an electrostatic generator that harnesses the motion of a living body," *JSME Int. J.*, ser. C, vol. 43, no. 4, pp. 916–922, 2000.

[20] W. J. Li, T. C. H. Ho, G. M. H. Chan, P. H. W. Leong, and H. Y. Wong, "Infrared signal transmission by a laser-micromachined vibration-induced power generator," in *Proc. 43rd IEEE Midwest Symp. Circuits and Syst.*, vol. 1, 2000, pp. 236–239.

[21] W. T. Thomson, *Theory of Vibration With Applications*, 4th ed. Englewood Cliffs, NJ: Prentice-Hall, 1993.

[22] R. Amirtharajah and A. P. Chandrakasan, "Self-powered low power signal processing," in *Proc. Tech. Dig. Papers Symp. VLSI Circuits*, 1997, pp. 25–26.

[23] M. J. Madou, *Fundamentals of Microfabrication*, 2nd ed. Boca Raton, FL: CRC, 2002.

[24] J. P. Den Hartog, "Forced vibrations with combined coulomb and viscous friction," *Applied Mechan. J. ASME*, vol. 53, pp. 107–115, Dec. 1931.

[25] E. S. Levitan, "Forced oscillations of a spring-mass system having combined coulomb and viscous damping," *J. Acoust. Soc. Amer.*, vol. 32, no. 4, pp. 1265–1269, Oct. 1960.

[26] P. D. Mitcheson, T. C. Green, E. M. Yeatman, and A. S. Holmes, "Analysis of optimized micro-generator architectures for self-powered ubiquitous computers," in *Adjunct Proc. UBICOMP 2002, 4th Int. Conf. Ubiquitous Computing*, Gothenburg, Sweden, Oct. 2002, pp. 5–6.

[27] P. Colwell, *Solving Kepler's Equation Over Three Centuries*. Richmond, VA: William-Bell, 1993.

[28] C. T.-C. Nguyen and R. T. Howe, "An integrated CMOS micromechanical resonator high-Q oscillator," *IEEE J. Solid-State Circuits*, vol. 34, pp. 440–455, Apr. 1999.

Paul D. Mitcheson (S'02) received the M.Eng. degree in electrical and electronic engineering from Imperial College, London, U.K., in 2001.

He is currently a Research Assistant with the Control and Power Research Group, Department of Electrical and Electronic Engineering, Imperial College. He is pursuing the Ph.D. degree focussing on micropower generators and associated power electronics.

Mr. Mitcheson is on the IEE London Younger Members Committee.

Tim C. Green (M'88–SM'01) received the B.Sc. degree in engineering (first class honors) from Imperial College, London, U.K., in 1986 and the Ph.D. degree in engineering from Heriot-Watt University, Edinburgh, U.K., in 1990.

He was a lecturer with Heriot Watt University until 1994 and is currently a Reader with Imperial College and a member of the Control and Power Research Group. His research interests include power electronics applied to generation and distribution of energy including issues of renewable and distributed generation, microgrids, power quality, active power filters, and flexible ac transmission systems.

Eric M. Yeatman (M'01) received the B.Sc. degree from Dalhousie University, Canada, in 1983, and the Ph.D. degree from Imperial College, London, U.K., in 1989.

Since then, he has been a Member of Staff in the Optical and Semiconductor Devices Group, Electrical and Electronic Engineering Department, Imperial College, currently as Reader and Deputy Head of Group. His research includes micromechanical actuators and generators, microstructures for microwave applications, and integrated optical amplifiers.

Andrew S. Holmes (M'02) received the B.A. degree in natural sciences from Cambridge University, U.K., in 1987, and the Ph.D. degree in electrical engineering from Imperial College, London, U.K., in 1992.

He is currently a Senior Lecturer with the Optical and Semiconductor Devices Group, Department of Electrical and Electronic Engineering, Imperial College. His research interests are in the areas of micropower generation and conversion, MEMS devices for microwave applications, and laser processing for MEMS manufacture.